Rev. LatinAm. Metal. Mat.

Artículo Regular

www.rlmm.org

SYNTHESIS, X-RAY DIFFRACTION AND MAGNETIC MEASUREMENTS OF $Cu(Ni,Co)_2InS_4$ ALLOYS: SUPERCONDUCTOR BEHAVIOR OF $CuCo_2InS_4$

Pedro Grima-Gallardo[1,2,3], Gerzon E. Delgado[4], Eduardo Pérez-Cappé[5], Jennifer Ann Aitken[6] and Dybia Prakash Rai[7].*

1: Centro de Estudios en Semiconductores (CES). Dpto. Física, Fac. Ciencias, Universidad de Los Andes (ULA), Mérida, Venezuela.
2: Centro Nacional de Tecnologías Ópticas (CNTO). Mérida. Venezuela.
3: Centro de Investigaciones de Astronomía (CIDA). Mérida. Venezuela.
4: Laboratorio de Cristalografía, Departamento de Química, Facultad de Ciencias, Universidad de Los Andes, Mérida, Venezuela.
5: Instituto de Ciencia y Tecnología de Materiales (IMRE), Universidad de La Habana, Vedado, Cuba.
6: Department of Chemistry and Biochemistry, Duquesne University, Pittsburgh, USA,
7: Department of Physics, Pachhunga University College, Aizawl, India-796001.

**e-mail: peg1952@gmail.com*

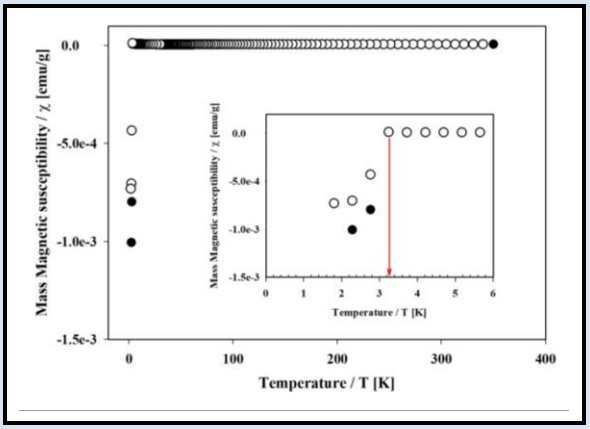

ABSTRACT

Polycrystalline samples of $CuCo_2InS_4$ and $CuNi_2InS_4$ alloys were prepared by the melt and anneal method. The products were characterized by X-Ray Diffraction (XRD) and Superconducting Quantum Interference Device (SQUID) techniques. From XRD it was found that both alloys, $CuCo_2InS_4$ and $CuNi_2InS_4$, are composed by two orthorhombic phases. In the case of $CuCo_2InS_4$, the crystal structure of the main phase has been refining (Rietveld method) as $Pmn2_1$ (N 31) with lattice parameters a=8.100(1) Å, b=7.116(8) Å and c=6.391(6) Å; for $CuNi_2InS_4$, the lattice parameters of the two phases were indexed (DICVOL 06). With respect to the magnetic behavior, $CuCo_2InS_4$ is a superconductor with Tc=3.2 K whereas $CuNi_2InS_4$ is a high temperature (Tc ~ 380 K) weak ferromagnetic with abnormal temperature dependence of the coercitive field.

Keywords: *Alloys, $CuCo_2InS_4$, $CuNi_2InS_4$, X-Ray diffraction, SQUID, superconductivity, ferromagnetism.*

SINTESIS, DIFFRACCIÓN DE RAYOS X Y MEDIDAS MAGNETICAS DE ALEACIONES DE $Cu(Ni,Co)_2InS_4$: COMPORTAMIENTO SUPERCONDUCTOR DE $CuCo_2InS_4$

RESUMEN

Las muestras policristalinas de las aleaciones $CuCo_2InS_4$ y $CuNi_2InS_4$ se prepararon mediante el método de fusión y recocido. Los productos se caracterizaron por las técnicas de difracción de rayos X (DRX) y dispositivo de interferencia cuántica superconductora (DIQUS). De los resultados de DRX se encontró que ambas aleaciones, $CuCo_2InS_4$ y $CuNi_2InS_4$, están compuestas por dos fases ortorrómbicas. En el caso de $CuCo_2InS_4$, utilizando el método de refinamiento Rietveld, se pudo determinar que la estructura cristalina de la fase principal pertenece al grupo espacial $Pmn2_1$ (N 31), con parámetros de la red a=8.100(1) Å, b=7.116(8) Å and c=6.391(6) Å; para $CuNi_2InS_4$, se indexaron los parámetros de las redes de ambas fases (principal y secundaria). Con respecto al comportamiento magnético, $CuCo_2InS_4$ es superconductor con Tc=3.2 K, mientras que $CuNi_2InS_4$ es un ferromagnético débil con Tc ~380 K con un comportamiento anómalo del campo coercitivo con la temperatura.

Palabras Claves: *Aleaciones, $CuCo_2InS_4$, $CuNi_2InS_4$, difracción de rayos X, DIQUS, superconductividad, ferromagnetismo.*

Recibido: 22-01-2020 ; **Revisado:** 21-04-2020
Aceptado: 15-05-2020 ; **Publicado:** 07-11-2020

pISSN: 0255-6952 | eISSN: 2244-7113
Rev. LatinAm. Metal. Mat. 2020; **40** (2): 131-141

DOI: *10.5281/zenodo.7603903*

1. INTRODUCTION

Diluted magnetic semiconductors (DMS) have been largely investigated due to their magnetic properties arising from the presence of magnetic ions in the atomic lattice [1]. The DMS compounds generally are obtained from solid solutions between semiconductors which contain one or more magnetic atoms in such a way that an average number of four valence electrons per atomic site and a value eight for the ratio valence electros to anions are maintained [2-3].

In the case of I-II_2-III-VI_4 compounds they belongs to the $(I\text{-}III\text{-}VI_2)_{1-x}$ $(II\text{-}VI)_x$ alloys family with x=2/3 (see Figure 1). In the early stage of the investigation on these compounds, Zn and Cd were often used as II-Type atom for the substitution of an I-III pair of atoms. In the classic book of Shay & Wernick [4] there is a list of twenty compounds with the disordered cubic zincblende or hexagonal wurzite crystal structures. More recently, it was found that $CuFe_2(Al,Ga,In)Se_4$ [5-6], $CuTa_2InTe_4$ [7] and $AgFe_2GaTe_4$ [8] crystallize in the stannite structure, with tetragonal space group $I\bar{4}2m$ (N 122) whereas $AgCd_2GaS_4$ [9] and $AgCd_2GaSe_4$ [10] have been reported with an hexagonal wurtz-stannite structure, orthorhombic space group $Pmn2_1$(N 31).

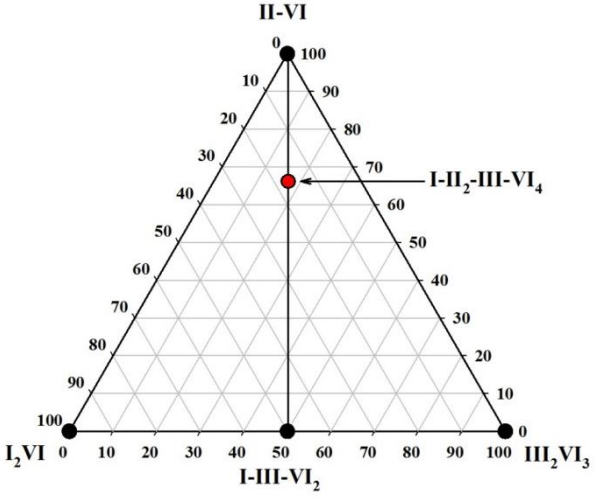

Figure 1. Ternary representation of the I-II_2-III-VI_4 compounds as members of the more general $(I\text{-}III\text{-}VI_2)_{1-x}$ $(II\text{-}VI)_x$ alloys family with x=2/3.

Due to the great variety of possible combinations (I: Cu, Ag; II: Zn, Cd, Hg, Mn, Fe, Co, Ni; III: Al, Ga, In; VI: S, Se, Te), these quaternary diamond-like materials can be useful for applications such as tunable semiconductors [11], photovoltaics [12], spintronics [13], non-linear optics [14] and themoelectrics [15].

In this work we report the preparation, lattice parameters and magnetic behavior of $CuCo_2InS_4$ and $CuNi_2InS_4$.

2. EXPERIMENTAL PART

2.1 Preparation of the samples

$CuCo_2InS_4$ and $CuNi_2InS_4$ samples were synthetized using the melt and anneal method [16]. Stoichiometric quantities of the elements with purity of 99.99% were charged in an evacuated synthetic silica glass ampoule that was previously subjected to pyrolysis in order to avoid the reaction of the starting materials with silica glass. Then, the ampoule was sealed under vacuum (10-3 Torr) and the fusion process was carried out inside a furnace (vertical position) heated up to 1500 K at a rate of 20 K/h with a stop of 48 h at 388 K (melting temperature of S) in order to maximize the formation of binary species at low temperature and minimize the presence of unreacted S at high temperatures. The ampoule was shaken using a mechanical system during the entire heating process in order to aid the complete mixing of all the elements. The maximum temperature (1500 K) was held for an additional 48 hours with the mechanical shaking system on. Then, the mechanical shaking system was turning off and the temperature was gradually lowered, at the same rate of 20 K/h, until 873 K. The ampoule was held at this temperature for a period of 30 days. Finally, the sample was cooled to room temperature at a rate of 10 K/h. The obtained ingots were bright gray color and homogeneous to the eye.

2.2 Powder diffraction

A small amount of each compound was thoroughly ground in an agate mortar and pestle. X-ray powder diffraction patterns were recorded using a PANalytical X'Pert Pro MPD powder X-ray diffractometer operating in Bragg-Brentano geometry using $K\alpha$ radiation with an average wavelength of 1.51187 Å. A tube power of 45 kV and 40 mA was employed. A nickel filter was used in the diffracted beam optics and the data were collected with the X'Celerator one-dimensional silicon strip detector. A 0.25° divergent slit, a 0.5°

antiscatter slit, and a 0.02 rad soller slit were set at both the incident and diffracted beams. The scan range was from 10 to 100° 2θ with a step of 0.008° and a scan speed of 0.0106°/s in the case of $CuNi_2InS_4$; for $CuCo_2InS_4$ the scan range was 10 to 100° 2θ with the same step and scan speed that for $CuNi_2InS_4$.

2.3 SQUID

DC measurements were performed on a Quantum Design SQUID magnetometer equipped with a superconducting magnet able to produce fields up to 8 x 10^4 Oe. The samples in the form of powder were compacted with a piece of cotton inside the sample holder in order to prevent any movement of the sample during measurements. Magnetic susceptibility measurements were performed using the Zero Field Cooling (ZFC) - Field Cooling (FC) protocol in the temperature range of 2-400 K. ZFC consist in cooling the sample from the highest temperature to the lowest measuring temperature in a zero magnetic field. Then a static magnetic field (100 Oe) is applied and magnetization measured during warming up. FC measurement consists of cooling the sample and measuring the magnetization during heating (at the same rate that in the ZFC process) without removal of the field. Magnetization as a function of the applied magnetic field at a given temperature measurements were also performed for magnetic fields in the range $-7x10^4 < H < 7x10^4$ Oe and temperatures of 1.8, 50, 150 250 and 300 K.

3. RESULTS AND DISCUSSION

In Figures 2 and 3, the experimental diffraction patterns for $CuCo_2InS_4$ and $CuNi_2InS_4$ were displayed, respectively. The analysis of the diffraction patterns with software DICVOL06 [17] (see Tables 1 and 2) indicates that both alloys are composed by two phases which had been indexed in the orthorhombic system. The lattice parameters of $CuCo_2InS_4$ phase I, a = 8.090 ± 0.003 Å; b = 7.117 ± 0.002 Å; c = 6.336 ± 0.002 Å, are close to those obtained for $AgCd_2GaS_4$: a = 8.1460(4) Å, b = 6.8989(4) Å, c = 6.5932(5) Å [18] and $Cu_2MnGeSe_4$: a = 7.977 Å, b = 6.854 Å, c = 6.552 Å [19] which crystallize in the orthorhombic structure, space group *Pmn2₁*(N 31), suggesting that phase I belongs to the same space group. With respect to $CuCo_2InS_4$ phase II and $CuNi_2InS_4$ phases I and II, no analogous orthorhombic phases were found when using ICSD lattice parameters database [20] or when a search was made on Cu-S, In-S and Ni-S binaries in the Inorganic Material Database (AtomWork) [21].

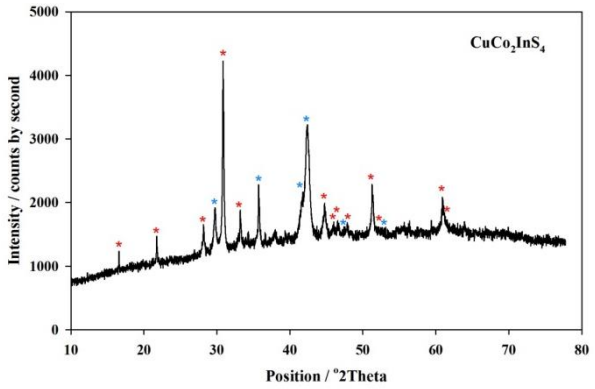

Figure 2. X-ray diffraction pattern of $CuCo_2InS_4$. Two phases were identified: phase I is denoted by red asterisks whereas phase II by blue asterisks.

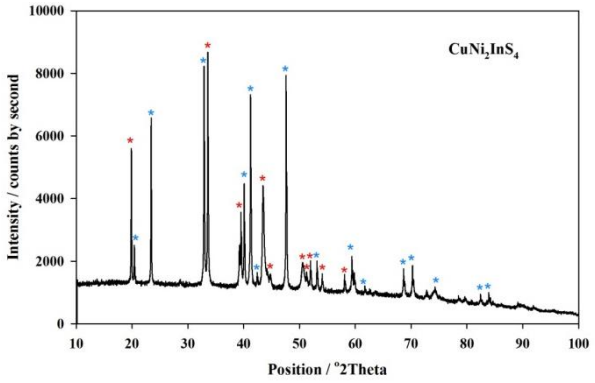

Figure 3. X-ray diffraction pattern of $CuNi_2InS_4$. Two phases were identified: phase I is denoted by red asterisks whereas phase II by blue asterisks.

Table 1. Indexation Table for $CuCo_2InS_4$. Phase I: Orthorhombic system. Lattice parameters: a = 8.090 ± 0.003 Å; b = 7.117 ± 0.002 Å; c = 6.336 ± 0.002 Å

	hkl	d_{obs} *[Å]*	d_{cal} *[Å]*	d_{obs}- d_{cal} *[Å]*	$2\Theta_{obs}$	$2\Theta_{cal}$	*Dif.* 2Θ
1	110	5.34185	5.34371	-0.00185	16.582	16.576	+0.006
2	111	4.07785	4.08494	-0.00709	21.777	21.739	+0.038
3	002	3.16591	3.16811	+0.00220	28.164	28.144	+0.020
4	012	2.89520	2.89431	+0.00089	30.860	30.870	-0.010
5	121		2.89699	-0.00179		30.840	+0.020
6	300	2.69700	2.69678	+0.00022	33.191	33.194	-0.003
7	400	2.02256	2.02259	-0.00002	44.773	44.773	+0.000
8	312	1.97395	1.97305	+0.00090	45.938	45.960	-0.022
9	231	1.94767	1.94736	+0.00031	46.594	46.602	-0.008
10	032	1.90011	1.89897	+0.00114	47.832	47.863	-0.031
11	040	1.77857	1.77928	-0.00072	51.329	51.307	+0.022
12	322		1.77863	-0.00007		51.327	+0.002
13	140	1.73732	1.73775	-0.00044	52.640	52.626	+0.014
14	114	1.51898	1.51873	+0.00024	60.944	60.955	-0.011
15	323	1.50597	1.50646	-0.00048	61.527	61.505	+0.022

Figures of merit: M (13) = 19.0; F(13) = 10.4 (0.0143, 87)

Phase II: Orthorhombic system. Lattice parameters: a = 9.017 ± 0.002 Å; b = 5.364 ± 0.002 Å; c = 3.659 ± 0.002 Å

	hkl	d_{obs} *[Å]*	d_{cal} *[Å]*	d_{obs}- d_{cal} *[Å]*	$2\Theta_{cal}$	$2\Theta_{obs}$	*Dif.* 2Θ
1	300	3.00618	3.00583	+0.00035	29.694	29.697	-0.003
2	211	2.51028	2.51068	-0.00040	35.740	35.734	+0.006
3	021	2.16359	2.16310	+0.00048	41.713	41.723	-0.010
4	311	2.13159	2.13137	+0.00022	42.369	42.374	-0.005
5	401	1.91939	1.91932	+0.00007	47.322	47.324	-0.002
6	321	1.75539	1.75574	-0.00034	52.057	52.046	+0.011

Figures of merit: M (6) = 86.3; F(6) = 31.8 (0.0061, 31)

Table 2. Indexation Table for $CuNi_2InS_4$. Phase I: Orthorhombic system. Lattice parameters: a= 10.807 ± 0.003; b= 9.778 ± 0.004; c= 3.180 ± 0.002

	hkl	d_{obs} [Å]	d_{cal} [Å]	d_{obs}- d_{cal} [Å]	$2\Theta_{obs}$	$2\Theta_{cal}$	Dif. 2Θ
1	120	4.45627	4.45420	+0.00207	19.908	19.917	-0.009
2	021	2.66510	2.66540	-0.00029	33.600	33.596	+0.004
3	031	2.27706	2.27590	+0.00116	39.545	39.566	-0.021
4	430	2.07839	2.07996	-0.00157	43.508	43.473	+0.035
5	411	2.01501	2.01462	+0.00039	44.950	44.959	-0.009
6	530	1.80167	1.80125	+0.00042	50.624	50.637	-0.013
	600		1.80111	+0.00056		50.641	-0.017
7	501	1.78681	1.78745	-0.00064	51.075	51.055	+0.020
8	601	1.77226	1.77130	+0.00096	51.525	51.555	-0.030
9	511	1.75797	1.75831	-0.00034	51.975	51.964	+0.011
10	620	1.69016	1.69006	+0.00010	54.227	54.231	-0.004
11	450	1.58411	1.58409	+0.00002	58.191	58.192	-0.001

Figures of merit: M(11) = 19.5; F(11) = 11.2 (0.0141, 70)

Phase II: Orthorhombic system. Lattice parameters: a= 12.658 ± 0.003; b= 11.944 ± 0.002; c= 5.430 ± 0.001

	hkl	d_{obs} [Å]	d_{cal} [Å]	d_{obs}- d_{cal} [Å]	$2\Theta_{obs}$	$2\Theta_{cal}$	Dif. 2Θ
1	220	4.33958	4.34344	-0.00387	20.449	20.431	+0.018
2	130	3.79520	3.79776	-0.00256	23.421	23.405	+0.016
3	002	2.71645	2.71487	-0.00021	32.969	32.966	+0.003
4	222	2.30223	2.30215	+0.00008	39.095	39.096	-0.001
5	032	2.24280	2.24299	-0.00019	40.175	40.171	+0.004
	312		2.24247	+0.00032		40.181	-0.006
6	051	2.18649	2.18647	+0.00002	41.256	41.256	0.000
7	322	2.13299	2.13254	+0.00045	42.340	42.349	-0.009
8	450	1.90687	1.90651	+0.00036	47.652	47.661	-0.009
9	213	1.72196	1.72197	-0.00001	53.146	53.146	0.000
	640		1.72297	-0.00101		53.112	+0.034
10	262	1.55562	1.55603	-0.00041	59.362	59.345	+0.017
11	470	1.50208	1.50182	+0.00025	61.704	61.716	-0.012

12	353	1.36506	1.36500	+0.00005	68.707	68.710	-0.003
	613		1.36466	+0.00040		68.730	-0.023
13	623	1.33833	1.33869	-0.00037	70.279	70.257	+0.022
	760		1.33846	-0.00013		70.271	+0.008
14	363	1.27646	1.27639	+0.00007	74.237	74.242	-0.005
15	823	1.16815	1.16820	-0.00005	82.511	82.506	+0.005
16	083	1.15173	1.15169	+0.00004	83.952	83.956	-0.004
	780		1.15126	0.00047		83.994	-0.042
	942		1.15210	-0.00037		83.919	+0.033

Figures of merit: M(16) = 14.0; F(16) = 6.1 (0.0072, 368)

For the alloy $CuCo_2InS_4$, Rietveld refinement method was used in order to verify the previous analysis; results are showed in Figures 4 to 6 and Tables 3 and 4.

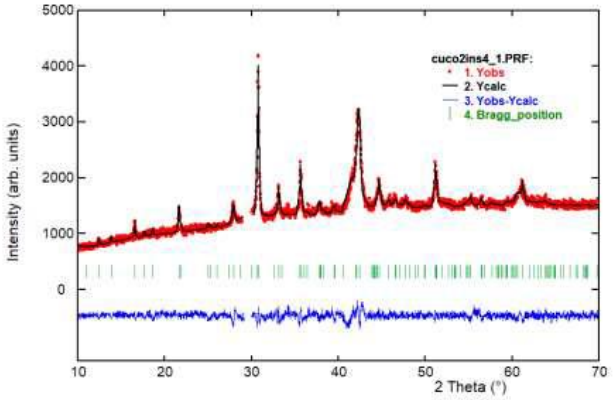

Figure 4. Final Rietveld plot showing the observed calculated and difference pattern for the $CuCo_2InS_4$ compound. The Bragg reflections are indicated by vertical bars. The peak in 2θ=29.697, was omitted for carried out the refinement

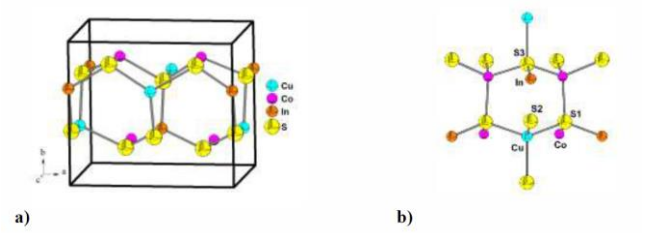

Figure 5. a) Unit cell diagram of $CuCo_2InS_4$ viewed in the *ba* plane and b) tetrahedral environment of the cation and anions in the crystal structure

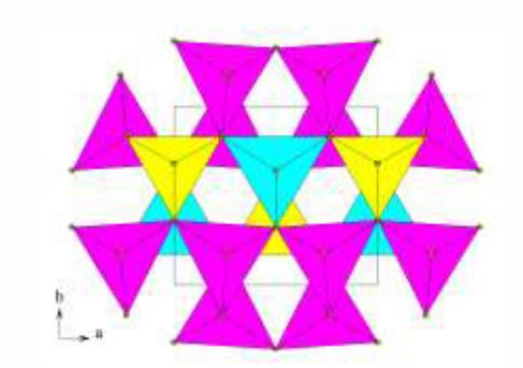

Figure 6. Crystal structure unit cell projection of $CuCo_2InS_4$ showing the tetrahedral array of cation-anion elements CuS_4 (cyan), CoS_4 (purple) and InS_4 (yellow).

Table 3. Results of Rietveld refinement for $CuCo_2InS_4$

Molecular formula	$CuCo_2InS_4$	D_{cal}	3.83 (g/cm^3)
Molecular weight	424.5 (g/mol)	*Z*	2
Crystal system	Orthorhombic	*Peak-shape profile*	Pseudo-Voigt
Space group	$Pmn2_1$ (N^o 31)		
a	8.100(1) Å	R_{exp}	2.7%
b	7.116(8) Å	R_p	3.3%
c	6.391(6) Å	R_{wp}	4.6%
V	368.4(5) Å^3	*S*	2.9

R_{exp} = 100 [(N-P+C) / $\sum_w(yobs^2)$]$^{1/}$2; *Rp* = 100 $\sum|y_{obs} - y_{calc}| / \sum|y_{obs}|$; R_{wp} = 100 $[\sum_w|y_{obs} - y_{calc}|^2 / \sum_w|y_{obs}|^2]^{1/2}$; $S = [R_{wp} / R_{exp}]$

N-P+C is the number of degrees of freedom

Table 4. Atomic coordinates, occupancy factors, isotropic temperature factor and bond distances (Å) for $CuCo_2InS_4$

Atom	*Ox.*	*Wyck.*	*x*	*y*	*z*	*foc*	*B (Å^2)*
Cu	+1	2a	0	0.335(5)	0.505(6)	1	0.9(7)
Co	+2	4b	0.251(5)	0.825(6)	0.510(6)	1	0.9(7)
In	+4	2a	½	0.324(5)	0.505(6)	1	0.9(7)
S1	-2	4b	0.265(5)	0.173(5)	0.395(5)	1	0.9(7)
S2	-2	2a	0	0.676(6)	0.360(5)	1	0.9(7)
S3	-2	2a	½	0.634(6)	0.395(5)	1	0.9(7)
Cu-S1		2.54(4)	Co-S1^{iii}	2.59(6)	In-S1		2.30(4)
Cu-S1^i		2.54(4)	Co-S1^{ii}	2.46(5)	In-S1^{iv}		2.30(4)
Cu-S2		2.60(6)	Co-S2	2.49(5)	In-S1^{ii}		2.32(6)
Cu-S3^{ii}		2.50(5)	Co-S3	2.54(5)	In-S3		2.27(5)

Symmetry codes: (i) -x, y, z; (ii) 0.5-x, 1-y, 0.5+z; (iii) x, 1+y, z; (iv) 1-x, y, z.

From that crystal structure refinement, it can be confirmed that $CuCo_2InS_4$ crystallize in the wurtzite-stannite symmetry, space group $Pmn2_1$ (N 31). This structure can be described as a hexagonal, closest-packed array of sulfur anions with Cu+, Co2+ and In4+ occupying tetrahedral holes, and is characterized by a three-dimensional arrangement of slightly distorted CuS_4, CoS_4 and InS_4 tetrahedra connected by corners. All S atoms are surrounded by two Cu atoms, one Co and one In atom, and each cation is coordinated by 4 anions (please see Figures 5 and 6). The fitted lattice parameters *a*=8.100(1) Å, *b*=7.116(8) Å and *c*=6.391(6) Å agrees well with *a* = 8.090 ± 0.003 Å; *b* = 7.117 ± 0.002 Å; *c* = 6.336 ± 0.002 Å obtained from indexation.

Only one peak cannot be refined (at 2Θ=29.697) which surely becomes from a secondary or impurity phase.

With respect to the alloy $CuNi_2InS_4$, until now, we are not found a model that describes with acceptability the experimental diffraction pattern.

The mass magnetic susceptibility of $CuCo_2InS_4$ is show in Figure 7. The behavior is typical of a superconductor i.e. nearly cero magnetic susceptibility in the entire temperature range and an abrupt transition to diamagnetic behavior at low temperature. The critical temperature (T_c) is ~3.2 K as it can be seen in the inset of Fig. 7.

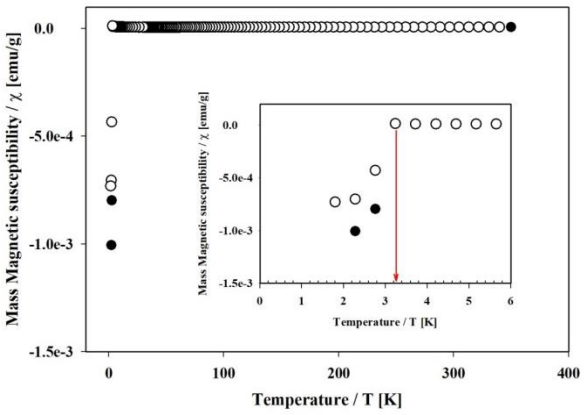

Figure 7. Mass magnetic susceptibility (χ) of $CuCo_2InS_4$. White circles: Zero Field Cooling (ZFC); black circles: Field Cooling (FC). The insert is a magnification of the low temperature range. The red arrow signals the critical temperature, T_c.

Superconductors can conduct electricity with no resistance below its critical temperature (T_c). One of the highest T_c has been observed in Cu-based high temperature superconductors (HTS) [22], 133 K at ambient pressure [23] and 164 K at high pressures [24]; however, the nature of the origin of superconductivity for these compounds has still not been explained. In contrast, the Bardeen-Cooper-Schrieffer (BCS) theory establish that a favorable combination of high frequency phonons, strong electron-phonon coupling and high density of states is a guide to achieving superconductivity; effectively, it has been proposed that these conditions can be fulfilled for metallic hydrogen and covalent compounds dominated by hydrogen [25-26] but although calculations predict critical temperatures between 50 and 235 K for many hydrides [27] only a moderate T_c~17 K has been observed experimentally [28]. In contrast, a T_c=203 K has been obtained experimentally in H_2S at ~100 GPa [29].

In the case of chalcopyrite alloys, this is the second time that we observe superconductivity. Previously we reported a T_c~11 K for the alloy $CuNbInTe_3$ [30] an alloy with monoclinic crystal structure where Te-atoms are tetra-coordinated and located in two planes in the unit cell, one at the top and one in the bottom of the monoclinic parallelepiped separated by a cation-plane at the center of the unit cell. This disposition is somewhat similar to that observed in HTS where a conducting layer interacts with a charge reservoir layer. In the case of $CuCo_2InS_4$, we observe two orthorhombic phases and at this stage of the investigation the attribution of the superconductor state to one of these phases would be only speculative; also, further scanning electron microscopy (SEM) measurements were desirable to discard the presence of segregation of elements or phases could be not observed in the diffraction patterns.

In Figure 8, mass magnetic susceptibility measurements on $CuNi_2InS_4$ are displayed. In this case we observe a weak ferromagnetic behavior with a critical temperature (the paramagnetic-ferromagnetic transition temperature) T_c ~ 350 K. At low temperature the curves show an exponential increase of the susceptibility which is due to the presence of a paramagnetic component superposed to the ferromagnetic one. Another feature is the hysteresis between zero field cooling (ZFC) and field cooling curves indicative of magnetic clusters formation.

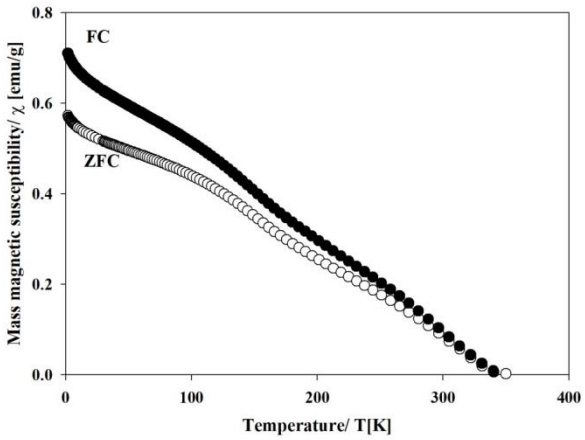

Figure 8. $CuNi_2InS_4$: Mass magnetic susceptibility (χ). Black circles: field cooling (FC). White circles: zero field cooling (ZFC).

In Figure 9, the magnetization is measured as function of the applied magnetic field at T=1.8, 150, 200, 250 and 300 K. From these curves, it can be obtained the magnetic saturation M_s, the magnetic remanence M_r and the coercitive field H_c. Following the temperature sequence of the curves it can be observed that: a) from T=1.8 K to T=300 K, the typical "S" shape of a ferromagnetic material tends to a right line typical of a paramagnetic; b) in the curve at T=1.8 K, the magnetic saturation was not achieved even at 7 x 10^4 Oe because of the presence of a relative low paramagnetic component as it was

stated in the previous paragraph; and c) the remanent magnetization (M_r) decreases with temperature (please, see Figure 10) and takes the zero value at T~ 380 K in concordance with the magnetic susceptibility curve (Figure 8).

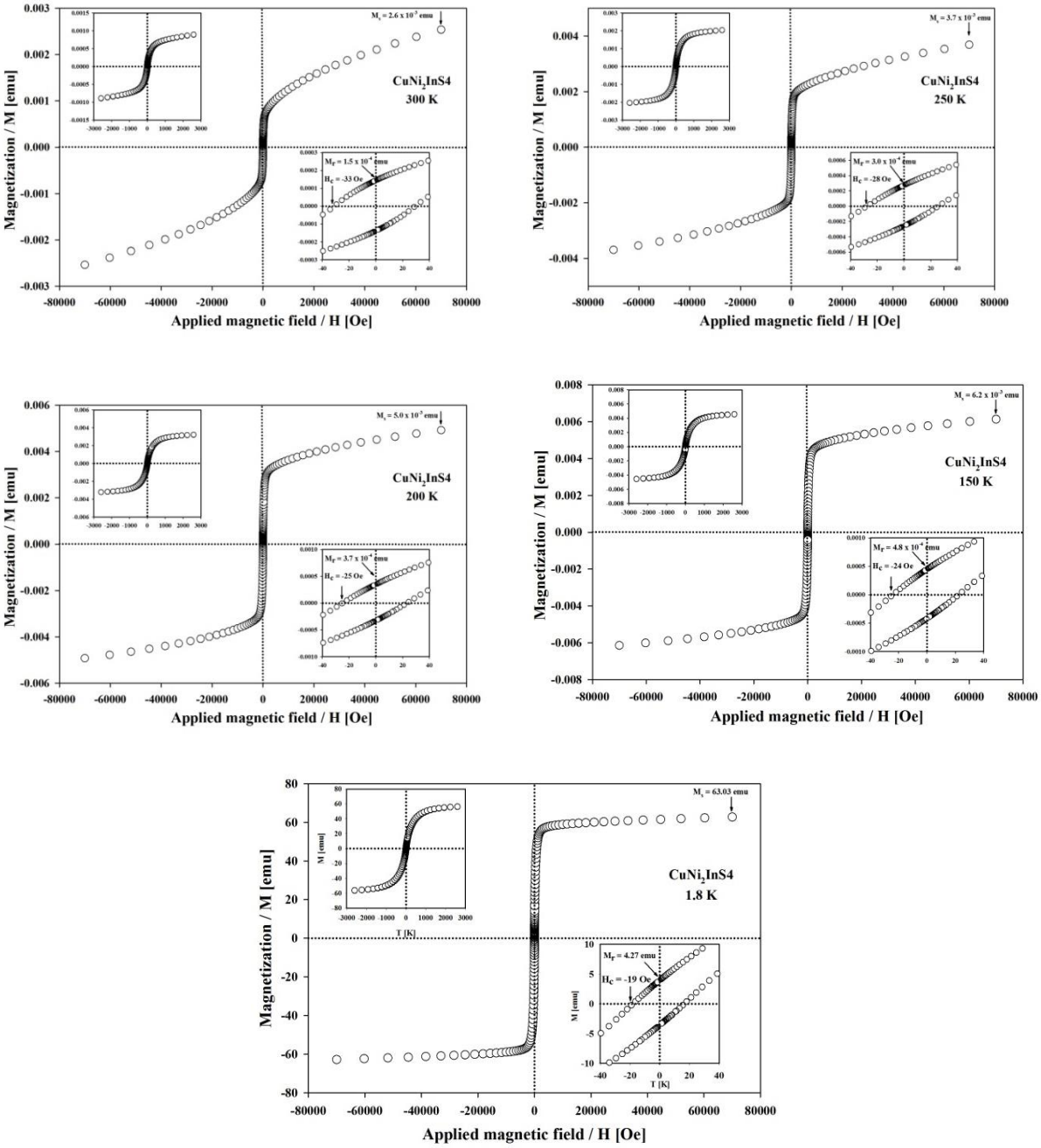

Figure 9. $CuNi_2InS_4$: Magnetization (M) vs magnetic field (H) at temperatures of 1.8, 150, 200, 250 and 300 K. The insets are amplifications at low magnetic fields.

The dependence of the coercitive field (H_c) with temperature (T) is displayed in Figure 11. The red circles correspond to + H_c whereas the black circles to - H_c. The relative shift of red and black circles indicates a deviation of the symmetry around H=0. i.e. the hysteresis curve is leger displaced to the left side. However, the most interesting behavior of this curve is the positive coefficient of H_c with T. Permanent magnets with a positive coefficient of coercitivity have gained intense research due to the

demand of the applications in the traction motors of hybrid and pure electric vehicles, microwave devices, and magnetic recording media, which need work under the varying temperature environment [31].

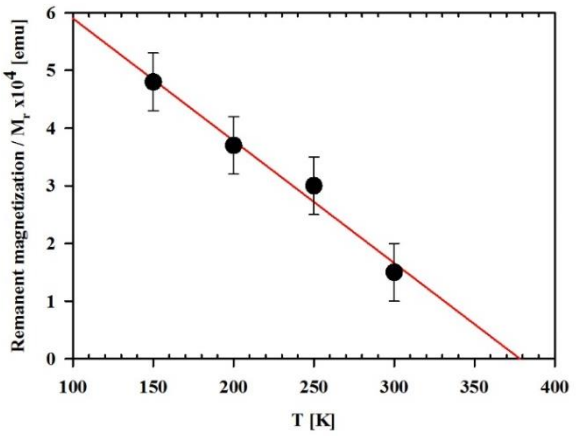

Figure 10. $CuNi_2InS_4$: Remanent magnetization (M_r) vs temperature (T). The red line is a linear fit over the experimental points.

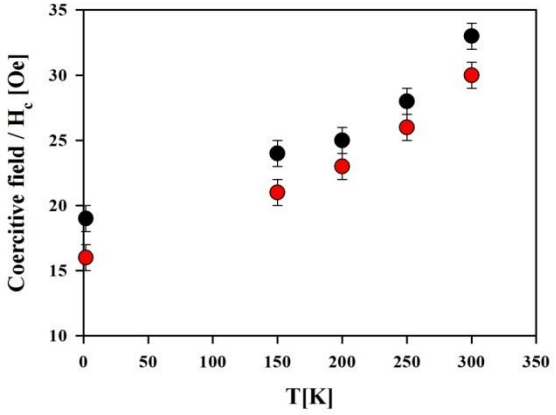

Figure 11. $CuNi_2InS_4$: Absolute value of the coercitive field (H_c) as a function of temperature (T). Black circles: $-H_c$; red circles: $+H_c$.

This abnormal temperature dependence of the coercitive field has been observed previously in $Sm_{1-x}Dy_x(Co_{0.695}Fe_{0.2}Cu_{0.08}Zr_{0.025})_{7.2}$ alloys [31] and $Sm(Co, Fe, Cu, Zr)_z$ powders [32], and it has been proposed that it is related to microstructure, cellular structure, especially controlled by the magnetic properties of cell boundary phase. In our case we speculate that it can be produced by the interaction of the two magnetic phases presented in the alloy. However, this conclusion must be confirmed by the study of other alloys of the system $(CuInS_2)_{1-x}(NiS)_x$ with compositions close to x=2/3 (which is the composition of $CuNi_2InS_4$), magnetic measurements of H_c vs T, and also investigation of the microstructure by TEM analysis.

4. CONCLUSIONS

$CuCo_2InS_4$ and $CuNi_2InS_4$ alloys were prepared and characterized by X-ray diffraction and magnetic susceptibility measurements. It was found that both alloys are composed by two orthorhombic phases. In the case of $CuCo_2InS_4$, the main phase has lattice parameters very close to $AgCd_2GaS_4$ and $Cu_2MnGeSe_4$ and crystallizes in the orthorhombic structure, space group *Pmn2₁* (N 31); for the secondary phase it cannot be possible obtain the space group because there are not enough experimental peaks. In the case of $CuNi_2InS_4$ the two phases have close lattice parameters which suggest the possibility of spinodal decomposition. From the magnetic measurements, it was found that $CuCo_2InS_4$ show superconductor behavior with Tc = 3.2 K and that $CuCo_2InS_4$ is a weak high temperature ferromagnet (Tc ~ 380 K) with abnormal temperature dependence of the coercitive field.

5. REFERENCES

[1]. Nikiforov KG. Prog. Crystal Growth Charac. Mater. 1999; 39: 1-104

[2]. Parthé E, Wurtzite, Sphalerite Structures. In: Westbrook J.H. & Fleischer R.L. (Eds) Intermetallic compounds, principles and applications, Vol. 1, John Wiley & Sons, Chichester, UK, 1995, Chap. 14.

[3]. Delgado JM. Inst. Conf. Series 1998; 152: 45-50.

[4]. Shay JL, Wernick JH. Ternary Chalcopyrite Semiconductors: Growth, Electronic Properties and Applications. Pergamon Press, Oxford, 1974, p.14.

[5]. Delgado GE, Mora AJ, Grima-Gallardo P, Quintero MJ. Alloys and Comp. 2008; 454(1-2): 306-309.

[6]. Delgado GE, Mora AJ, Grima-Gallardo P, Muñoz M, Durán S, Quintero M. Bull. Mater. Science. 2015; 38(4): 1061-1064.

[7]. Delgado GE, Mora AJ, Grima-Gallardo P, Muñoz M, Durán S, Quintero M. Phys. B Cond. Matter. 2008; 403(18): 3228-3230.

[8]. Delgado GE, Quintero E, Tovar R, Grima-Gallardo P, Quintero MJ. Alloys and Comp. 2014; 613: 143-145.

[9]. Chykhrij SI, Parasayuk OV, Husak OA, Kadykalo EM. J. Alloys and Comp. 2000; 312(1-2): 189-195.

[10]. Olekseyuk ID, Gulay LD, Parasayuk OV, Husak OA, Kadykalo EM. J. Alloys and Comp. 2002;

343(1-2): 125-129.

[11]. Ford GM, Guo Q, Agrawal R, Hillhouse HW, Hugh W. Chemistry of Materials 2011; 23(10): 2626-2629.

[12]. Guo Q, Ford GM, Yang WC, Walker BC, Stach EA, Hillhouse HW. J. American Chem. Soc. 2010; 132 (49): 17384-17386.

[13]. Chambers SA, Yoo YK. MRS Bulletin 2003; 28: 706-710.

[14]. Li Y, Fan W, Sun H, Cheng X, Li P, Zhao X. J. Phys. Cond. Matter. 2011; 23(22): 225401.

[15]. Sevik C., Çağin T. Phys. Rev. 2010; B82(4): 045202.

[16]. Grima-Gallardo P, Méndez L, Delgado GE, Cabrera H, Pérez-Cappé E, Zumeta-Dubé I, Rodríguez A, Aitken JA, Rai DP. Int. J. Exp. Spectroscopy 2018; 3:016.

[17]. D. Louer, A. Boultif. http://www.ccp14.ac.uk/solution/indexing/index.html.

[18]. Chykhrij SI, Parasyuk OV, Halka VO. J. Alloys and Comp. 2000; 312(1):189-195; Olekseyuk ID, Gulay LD, Parasyuk OV, Husak OA, Kadykalo EM. J. Alloys and Comp. 2002; 343(1-2):125-131; Pervukhina NV, Atuchin VV, Parasyuk O. Acta Cryst. 2005; E61: i91-i93.

[19]. Guen L, Glaunsinger WS. J. Solid State Chemistry 1980; 35: 10-21.

[20]. https://www.icsd.fiz-karlsruhe.de

[21]. http://crystdb.nims.go.jp

[22]. Bednorz JG, Mueller KA. Zeitschrift für Physik 1986; B64: 189-193.

[23]. Schilling A, Cantoni M, Guo JD. Nature 1993; 363: 56-58.

[24]. Gao L, Xue YY, Chen F, Xiong Q, Meng RL, Ramirez D, Chu CW, Eggert JH, Mao HK. Phys. Rev. 1994; B50: 4260-4263.

[25]. Ashcroft NW. Phys. Lett. 1968; 21: 1748-1750.

[26]. Ashcroft NW. Phys. Lett. 2004; 92: 187002.

[27]. Eremets MI, Trojan IA, Mendeved SA, Tse JS, Yao Y. Science 2008; 319: 1506-1509.

[28]. Drozdov AP, Eremets MI, Trojan IA. 2014; arXiv:1412.0460.

[29]. Drozdov AP, Eremets MI, Troyan IA, Ksenofontov V, Shylin SI. Nature 2015; 525: 73-76.

[30]. Grima-Gallardo P., Palmera M., Muñoz M., Durán S., Quintero M., Quintero E., Nieves L., Moreno E., Ramos M.A. and Romero H. Adv. Mat. Sci. & Technol. 2013; 7: 1-11.

[31]. Liu L., Liu Z., Li M., Lee D., Chen R.J., Liu J., Li W. and Yan R. Appl. Phys. Letts. 2015; 106: 052408.

[32]. Liu J.F., Chui T. and Hadjipanavis G.C. Appl. Phys. Lett. 1998; 73: 3007.